ADVANCED ELECTRONIC MATERIALS
www.advelectronicmat.de

Highly Sensitive Pressure Sensor Based on Bioinspired Porous Structure for Real-Time Tactile Sensing

*Subin Kang, Jaehong Lee, Sanggeun Lee, SeulGee Kim, Jae-Kang Kim, Hassan Algadi, Saleh Al-Sayari, Dae-Eun Kim, DaeEun Kim, and Taeyoon Lee**

A flexible pressure sensor with high performances is one of the promising candidates for achieving electronic skins (E-skin) related to various applications such as wearable devices, health monitoring systems, and artificial robot arms. The sensitive response for external mechanical stimulation is fundamentally required to develop the E-skin which imitates the function of human skin. The performance of capacitive pressure sensors can be improved using morphologies and structures occurring in nature. In this work, highly sensitive capacitive pressure sensors based on a porous structure of polydimethylsiloxane (PDMS) thin film, inspired on the natural multilayered porous structures seen in mushrooms, diatoms, and *spongia offilinalis*, have been developed and evaluated. A bioinspired porous dielectric layer is used, resulting in high-performance pressure sensors with high sensitivity (0.63 kPa^{-1}), high stability over 10 000 cycles, fast response and relaxation times, and extremely low-pressure detection of 2.42 Pa. Additionally, the resulting pressure sensors are demonstrated to fabricate multipixel arrays, thus achieving successful real-time tactile sensing of various touch shapes. The developed high-performance flexible pressure sensors may open new opportunities for innovative applications in advanced human-machine interface systems, robotic sensory systems, and various wearable health monitoring devices.

1. Introduction

Wearable devices have attracted a considerable amount of interest and increasing demand over the last decades, as revealed by the significant developments observed in diverse wearable technologies, including flexible devices,[1,2] textile electronics,[3,4] flexible displays,[5] and electronic skins (E-skin).[6–12] Among the technologies, E-skin, electronic devices which imitate the properties of natural human skin sensing network, has been widely explored for use in various applications such as smart prosthetics,[6] interactive wearable devices,[7,8] artificial robot arms,[9,10] and health monitoring systems.[11,12] For realizing such applications, tactile sensing abilities (responsiveness to external mechanical force) are fundamental to essentially emulate the function of the sensory receptors (mechanoreceptor, nociceptor) in human skin. Over the last few years, various types of pressure sensors including resistive,[13–16] capacitive,[17–19] piezoelectric,[20,21] and optical type[22] sensors have been intensively investigated as promising candidates for E-skin applications. In particular, capacitive type pressure sensors exhibit strong advantages in terms of its high sensitivity, low power consumption, simple design, and very fast response. To ensure the fabrication of high-performance capacitive pressure sensors, various approaches to fabricate the pressure sensors using microstructured dielectric layers[23] and utilizing air gap with spacer between electrodes[24] have been attempted. Mannsfeld et al. demonstrated pyramidal and line-structured microstructures which can be applicable to organic field effect transistors (OFETs), thus obtaining OFET-based pressure sensors.[25] In addition to the pyramidal microstructures, various other forms of micropatterned dielectric layers have been used to enhance the performance of pressure sensors, including pillars, domes, and wrinkle patterns.[26–29] Nevertheless, there still remain demands for highly sensitive and high-resolution pressure sensors exhibiting the sophisticated pressure sensing properties of human skin.

To achieve the improvement of the pressure sensors, considerable efforts to develop mechanical sensors with morphologies and structures inspired by natural living beings have been dedicated. Examples of this approach can be found, for instance, in a spider sensory system being used as model for a strain sensor,[30] a gecko's foot for a hierarchical array pressure sensor,[31] a *Margaritaria. nobilis* fruits photonic structure for an optical sensor,[32] and a human ear drum for an active membrane sensor.[33] In nature, there are some species such as *spongia officinalis*, diatoms and mushrooms that can be effectively deformed even by subtle pressure because of the porous structure of their organs. In the case of *spongia officinalis*, it

S. Kang, J. Lee, S. Lee, S. Kim, H. Algadi, Prof. D.-E. Kim, Prof. D. E. Kim, Prof. T. Lee
School of Electrical and Electronic Engineering
Yonsei University
50 Yonsei-ro, Seodaemun-Gu
Seoul 120-749, Republic of Korea
E-mail: taeyoon.lee@yonsei.ac.kr
J.-K. Kim, Prof. D.-E. Kim
School of Mechanical Engineering
Yonsei University
50 Yonsei-ro, Seodaemun-gu, Seoul 120-749, Republic of Korea
Prof. S. Al-Sayari
Promising Center for Sensors and Electronic Devices
Najran University
1988 Najran 11001, Saudi Arabia

DOI: 10.1002/aelm.201600356

has complex pore structures with high, hierarchically porosity ranging from the nanometer to the micrometer length scale which show high sensitivity and reversible compressibility, in spite of its light weight and low densities.[34,35] On the basis of the porous structure, the *spongia officinalis* has superb mechanical characteristic such as outstanding flexibility, softness, and resiliency, which are the main strength for acquiring high-performance pressure sensors.[36] Despite the existence of such abilities in nature, bioinspired capacitive pressure sensors mimicking natural porous structures have hitherto been largely overlooked.

In this research, we present and evaluated a facile approach to fabricate highly sensitive capacitive pressure sensor based on a sponge-like structure of polydimethylsiloxane (PDMS) thin-film dielectric layer. The morphology of the porous structured dielectric layer in the fabricated pressure sensors was controlled by changing the pore sizes. These flexible pressure sensors were capable of not only detecting extremely low pressures, but also of enabling real-time tactile sensing applications. The porous structured pressure sensor with 6 μm pore diameter exhibited high sensitivity (0.63 kPa^{-1}), high stability over more than 10 000 cycles of applied pressure, and fast response time (in the milliseconds range). This sensor was pixelated into a flexible 15 × 15 array, indicating that such sensors can be potentially applied on real-time tactile mapping systems. This highly sensitive pressure sensor based on a bioinspired porous structure may open a new gateway for applications in advanced human-machine interface systems.

2. Results and Discussion

Figure 1a shows a photograph of *spongia officinalis* which is better known as sponge and a schematic illustration of the overall fabrication process of porous structured pressure sensors. The sponge in nature (the photograph in Figure 1a) is mainly composed of hierarchically porous structured organs which enable the species to have greatly sensitive compressibility against a subtle external stimulation. The procedure to fabricate the *spongia officinalis* mimicked porous elastomeric film for high-performance pressure sensor involves three main steps: (i) stacking polymer microbeads on an

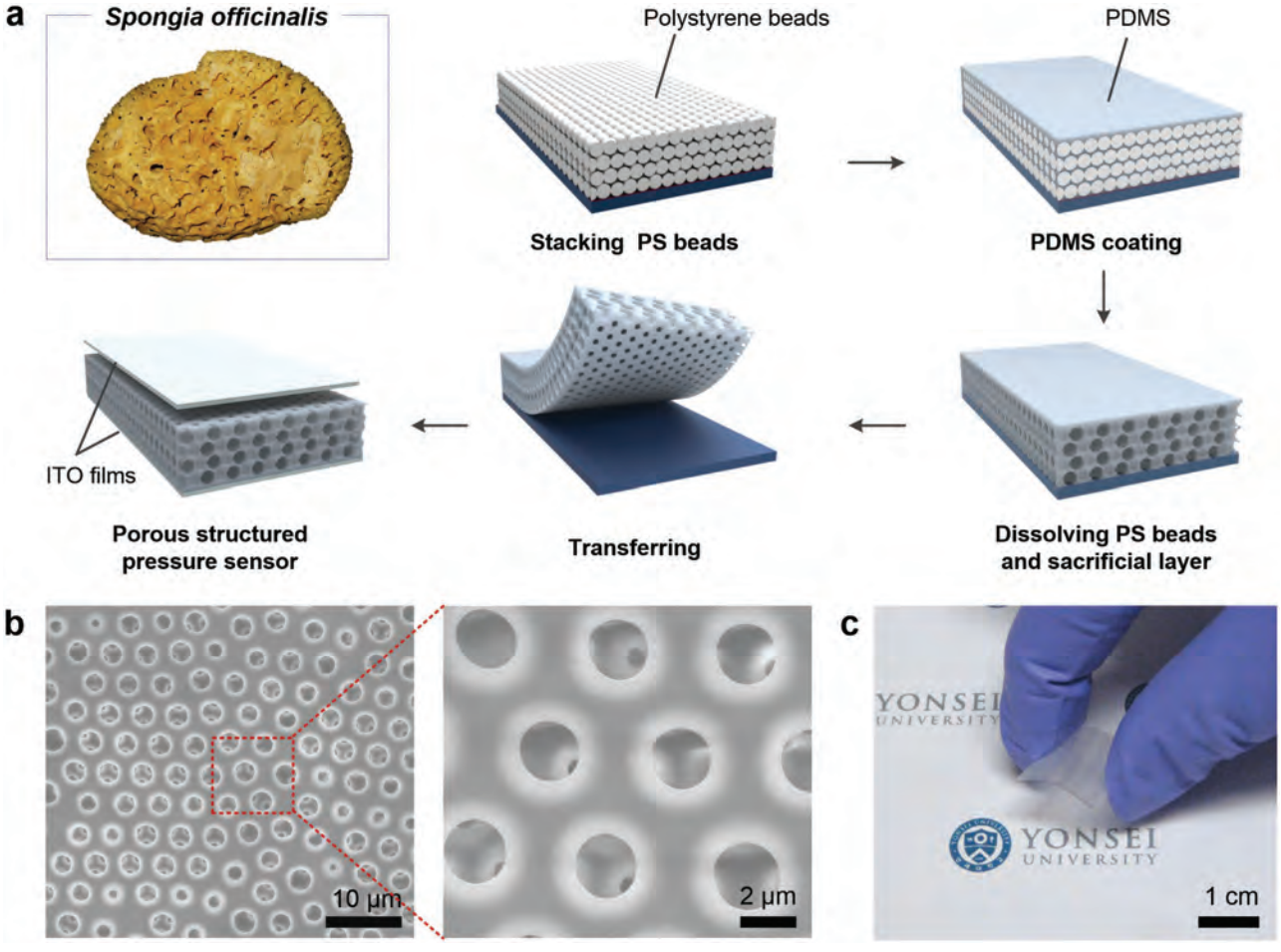

Figure 1. a) Photograph of a *Spongia officinalis* and schematic illustration of the fabrication steps of a porous structured capacitive pressure sensor. b) Top views of SEM images of a porous structured PDMS film fabricated using PS beads (diameter: 4 μm). The corresponding higher magnification image shows that the pores are uniformly formed in the multilayer configuration. c) Photograph of the fabricated porous structured pressure sensor with 1.5 × 1.5 cm ITO/PET films as electrodes.

Si substrate, (ii) coating a PDMS film on the microbeads stacked on the substrate, and (iii) dissolving the polymer beads and transferring the porous PDMS film onto the electrodes. To allow an easier and clearer transfer of the porous PDMS film as a dielectric layer, the Si substrate was coated with sacrificial layer before stacking the polymer microbeads. Having done that, multilayer of polystyrene (PS) beads were stacked on the substrate by dropcasting, with a face-centered cubic structure with of long-range order. As shown in Figure S1 (Supporting Information), the PS beads were uniformly stacked on the substrate; different diameters of PS microbeads were used in different sensors (2, 4, and 6 µm). The stacked PS beads were fully covered with the PDMS layer and then heated to cure this layer. To achieve the porous structured PDMS layer, the PS beads and the sacrificial layer were effectively etched by immersing the sample in an organic solution.[37] Figure 1b presents a typical scanning electron microscopy (SEM) images of the obtained inverse-opal-structured PDMS film, which shows that the multilayered porous structure of the PDMS film was successfully formed as detailed in the corresponding higher magnification image. Various porous PDMS films with different pore sizes were successfully fabricated, using different sizes of PS microbeads (Figure S2, Supporting Information). The uniform pores were formed without any residue of PS beads in the porous PDMS layer, which clearly indicates the complete removal of the polymer beads. Transferring the porous dielectric PDMS layer from the Si substrate onto an indium tin oxide (ITO)/polyethylene phthalate (PET) film to be used as an electrode, a highly sensitive porous structured pressure sensor was obtained. Figure 1c presents a photograph of the fabricated porous structured pressure sensor which is highly flexible.

The capacitance of capacitive pressure sensors can be calculated by $C = \varepsilon (A/d)$, where ε represents the permittivity of the dielectric layer, A and d are the area and the distance between the electrodes, respectively. The capacitance of a pressure sensor can be changed very effectively by applying external loads, which induces the change of the thickness of the porous dielectric layer and effective dielectric constant. **Figure 2**a provides the relative changes of capacitance in the pressure sensor based on 4 µm pore-sized PDMS dielectric layer, which were measured against increasing loads of 0.05, 0.1, and 0.3 N. The porous structured pressure sensors exhibited continuous and stable capacitive responses at the various loads. In addition, although the capacitive response of the unstructured (bare PDMS, with no pores) pressure sensor had considerable noise because of its poor response, all the porous structured pressure sensors of different pore sizes exhibited essentially noise-free responses and consistent increases in their relative capacitance change at the various loads, as shown in Figure S3 (Supporting Information). Figure 2b presents the capacitive responses of the various pressure sensors for the same external force (0.2 N), showing that the capacitive responses of the porous structured pressure sensors were considerably enhanced compared to the unstructured pressure sensor.

To quantitatively evaluate the performance of the porous structured pressure sensors, the relative change in capacitance for a linearly increasing pressure was measured (Figure 2c). The sensitivity of a capacitive type pressure sensor (S) is typically

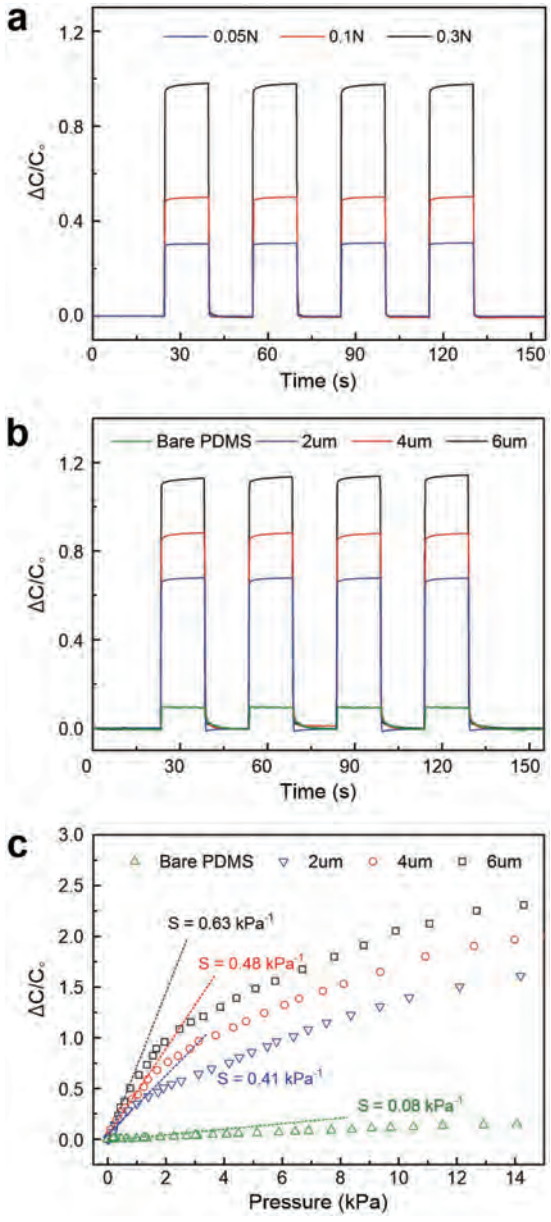

Figure 2. a) Response (capacitance variation) of the porous structured pressure sensor with 4 µm pores for the various applied loads of 0.05, 0.1, and 0.3 N. b) Response of the porous structured pressure sensors with different pore sizes of 2, 4, and 6 µm to a force of 0.2 N. c) Relative capacitance curves for the three different porous structured pressure sensors and the unstructured pressure sensor against increasing pressure. The maximum slope of relative capacitance change of the pressure sensor is 0.63 kPa^{-1} (for 6 µm pores).

defined as $S = \delta(\Delta C/C_0)/\delta p$, where p indicates the applied pressure, and ΔC and C_0 represent the capacitance change with the applied pressure and capacitance without the applied pressure, respectively. As shown in Figure 2c, a sensitivity of 0.63 kPa^{-1} was obtained for the porous structured pressure sensor with a 6 µm pore size in the low-pressure range (under 1 kPa), as determined by the graph slope. This value is comparable with that of the previously reported capacitive pressure sensors[19,23,38] and

considerably higher than the sensitivity of 0.08 kPa^{-1} obtained for the unstructured pressure sensor. This impressive enhancement in sensitivity of the porous structured pressure sensor is attributed to two key factors which are the presence of many spherical pores inside the PDMS films, making the dielectric layer significantly elastic, and the increase in the effective dielectric constant, resulting from the combined effect of both the PDMS dielectric constant ($\varepsilon_{PDMS} \approx 3.0$) and that of the air in the pores ($\varepsilon_{air} = 1.0$).[25] Specifically, the permittivity of the dielectric material in the pressure sensor is calculated by $\varepsilon = \varepsilon_0\varepsilon_r$, where ε_0 and ε_r refer to the space permittivity and relative dielectric constant of the dielectric material, respectively. In case of our porous structured pressure sensor, the effective relative dielectric constant, ε_r, can be estimated by $\varepsilon_r = \varepsilon_{air}P_{air}+\varepsilon_{PDMS}P_{PDMS}$, where P_{air} and P_{PDMS} refer the volume proportion of the air and PDMS in our porous structured PDMS layer film, respectively. When pressure is applied to our pressure sensor, the proportion of the air, which has lower permittivity, is decreased resulting in the increase of the effective permittivity of the dielectric layer and the capacitance of the pressure sensor. Therefore, the capacitive response of the porous structured sensor for external pressure can be effectively enhanced compared to the pressure sensor using unstructured PDMS. The capacitive response of the porous structured pressure sensor, therefore, significantly increased with the applied pressure not only as a result of the reduced distance between electrodes, but also because of the increase in the effective dielectric constant at the same time. In the high-pressure region (>1 kPa), a consecutive reduction in sensitivity was observed. Since the pores were already almost fully compressed, which is similar to the unstructured film, the dielectric layer had a lower effective elasticity. The sensitivity in this region is therefore considerably lower than in the low-pressure region.

The difference between sensitivities of the porous structured pressure sensors with different pore sizes is closely related to the compressibilities of the porous PDMS films. To evaluate the compressibilities of the films under external loads, the indentation depth profiles of the bare and porous PDMS films were measured with a homemade microindenter; the results are shown in **Figure 3**a. The almost identical loading and unloading curves of all films in the indentation profile indicate an elastic deformation and recovery of the samples. When a constant force was applied to the films, the indentation depths of the porous PDMS films were much deeper than that of the unstructured film, indicating that the porous structured PDMS dielectric layers were highly elastic compared with the unstructured film, regardless of pore size. The high compressibilities of the porous PDMS films were also confirmed by the lower stiffness, which generally means the extent to resist deformation against the applied loads and can be obtained by the slope of the graph in Figure 3a, of the porous PDMS films, when compared with that of the unstructured film. In particular, porous PDMS films with larger pore sizes exhibited higher compressibility (lower stiffness) than porous PDMS films with smaller pore sizes, as seen in Figure 3a. To analyze and compare the compressibility of the porous structures with different pore sizes, the unit support in the porous structure was simplified to an isotropic elastic half pillar. Sneddon provided a solution for the compliance, which is the inverse of the stiffness (and has units of meters per newton) of an isotropic elastic half pillar with a flat-ended punch indenting.[39] The Sneddon compliance ($C_{Sneddon}$) is given by

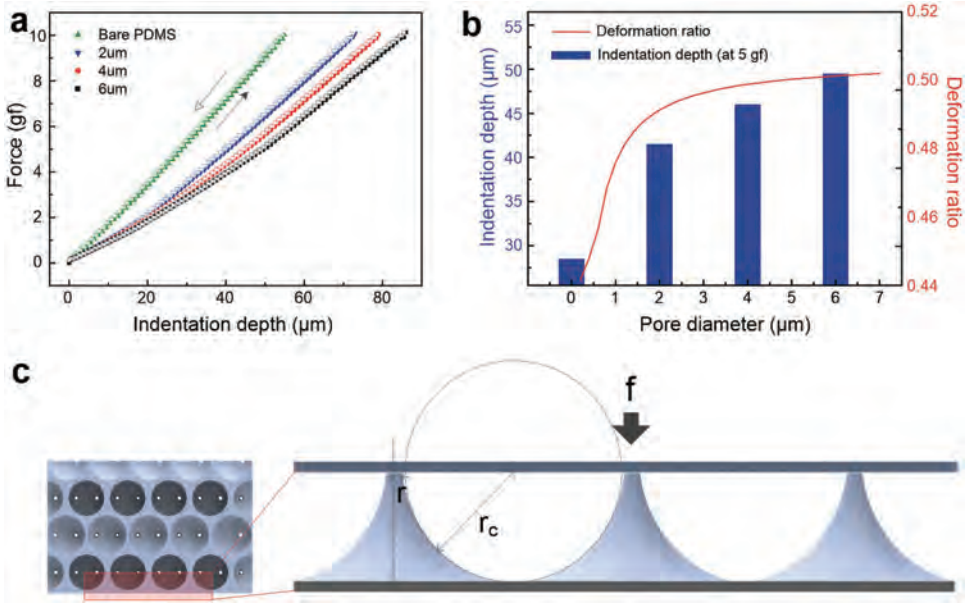

Figure 3. a) Microindentation depth profile for the unstructured and porous structured films. b) Relations between the experimental indentation depth and the theoretical deformation ratio of the porous structure according to the pore size. The red line represents the theoretically calculated deformation ratio of the porous films and the blue bars indicate the experimental indentation depth of porous structured films with respect to the pore sizes under an applied load (5 gf). c) Schematic illustration of the simplified model for the porous structure using cylindrical pillars when a force (*f*) is applied. *r* and r_c indicate the pillar radius and the fillet radius of the structure.

$$C_{\text{Sneddon}} = \frac{(1-\nu^2)}{2E\eta(r+r_c)} \quad (1)$$

where ν and E are the Poisson's ratio and elastic modulus of material, respectively, and η is a correction constant chosen to account for the complex geometry. The r and r_c parameters are respectively the pillar radius and fillet radius of the pillar. Based on Equation (1) which is equivalent to the reciprocal of the stiffness, the ratio of the compressed depth to the original thickness of the porous films under a constant external load (5 gf) was theoretically calculated according to the pore sizes of the films. Details of the theoretical estimation regarding the ratio are provided in the Supporting Information. Figure 3b provides the theoretical deformation ratio of the porous films with respect to their pore sizes and experimental results. The indentation depth measurement of the porous films with 2, 4, and 6 μm pore structures were obtained under a constant load of 5 gf, which resulted in 41.5, 46, and 49.5 μm, respectively. There was acceptable agreement between the theoretical tendency of the compressibilities and indentation depths of the various porous films. Therefore, it can be expected that the compressibility improvement of the porous structured films with larger pore sizes leads to a higher sensitivity of the resulting pressure sensors as shown in Figure 2c. In addition, when the same amount of external force was applied on the pressure sensor, the film with large pores showed larger deformation ratio than the smaller pore sized films and it concludes that the air inside the large pore was diminished earlier than the others. Moreover, our pressure sensors have the same thickness of the dielectric films and the porous structured pressure sensor has more pores as the pore size decreases. The applied pressure in each layer can be slightly reduced due to energy losses occurred between each layers. Therefore, as shown in Figure 2c, the pressure sensor with large pore size has diminished the pores earlier than the pressure sensors with smaller pores and shows a narrow workable range in high sensitivity than others.

To demonstrate the obtained outstanding sensitivity, the porous structured pressure sensor was shown to be capable of reliably detecting ultrasmall objects, by loading and unloading an ant (weight: ≈20 mg) as described in **Figure 4**a. The ant was placed on a porous PDMS pressure sensor (6 μm pore sizes) with a size of 0.9 × 0.9 cm; a rapid and distinguishable response was successfully obtained for both the placement and removal of the ant, which corresponds to a very tiny pressure of ≈2.42 Pa. Figure 4b shows the capacitive responses of the pressure sensors with and without a porous structure under a wide range of pressures. With high applied pressures of over 90 kPa, the difference between the capacitive responses of the porous and unstructured pressure sensors was much larger than in the low-pressure region, as expected. As can be seen in this figure, the porous PDMS pressure sensor effectively detects the applied pressure not only in the normal pressure range (region i) but also in the very high-pressure range (regions ii and iii), albeit with decreasing sensitivity. Figure 4c displays the relaxation and steady-state curves for the porous (6 μm pores)

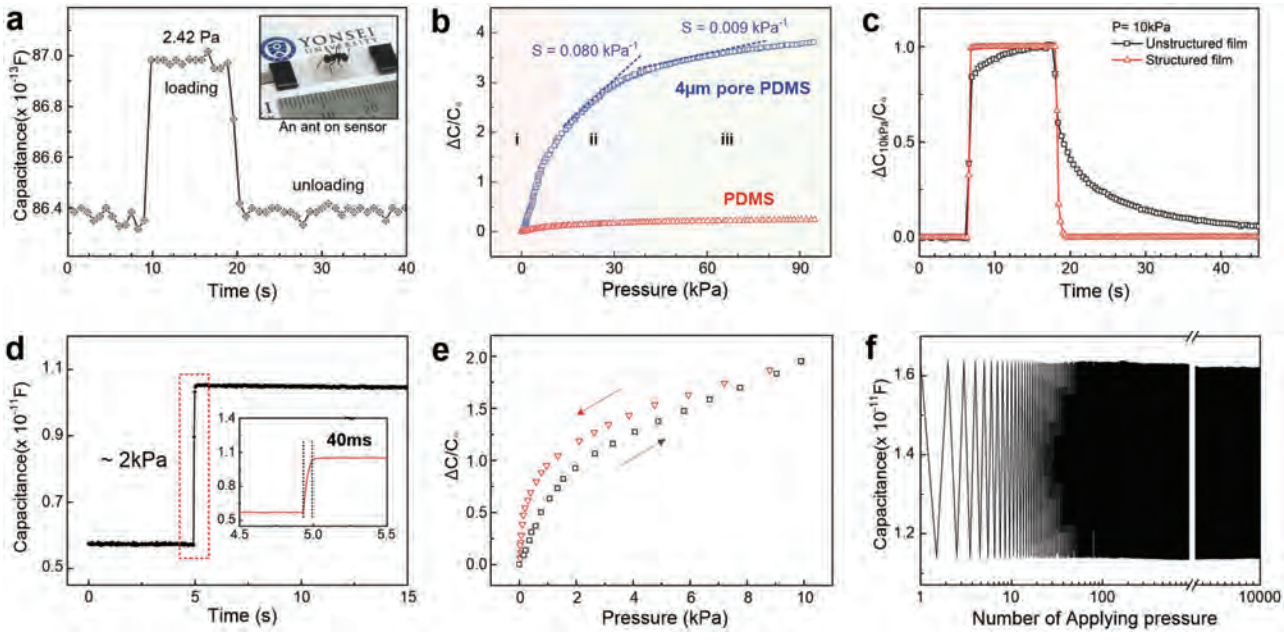

Figure 4. a) Response of the pressure sensor against loading and unloading of an ant (20 mg). The pressure applied by the ant is 2.42 Pa. (The inset shows the photograph of the ant on the 0.9 × 0.9 cm porous structured pressure sensor with 6 μm pore.) b) Relative capacitance change for a linearly increasing applied pressure, up to pressures in excess of 90 kPa. The pressure region can be divided into three regions. The low pressure range (region i) shows the high sensitivity and the high pressure ranges (regions ii and iii) show that the sensitivities decrease as progressively increasing pressure. c) Relaxation and steady-state curves for porous structured (6 μm) and unstructured pressure sensor to loading and unloading (10 kPa for 12 s). d) Capacitive response of porous structured pressure sensor with 4 μm for loading 2 kPa. Inset displays a capacitive response time (≈40 ms) with the millisecond range. e) Relative capacitance change of the porous structured pressure sensor with 6 μm pore size during a continuous loading and unloading cycle of pressure. f) Durability and stability of the pressure sensor response over 10 000 cycles, with a 0.5 N load.

ADVANCED ELECTRONIC MATERIALS
www.advelectronicmat.de

Materials Views
www.MaterialsViews.com

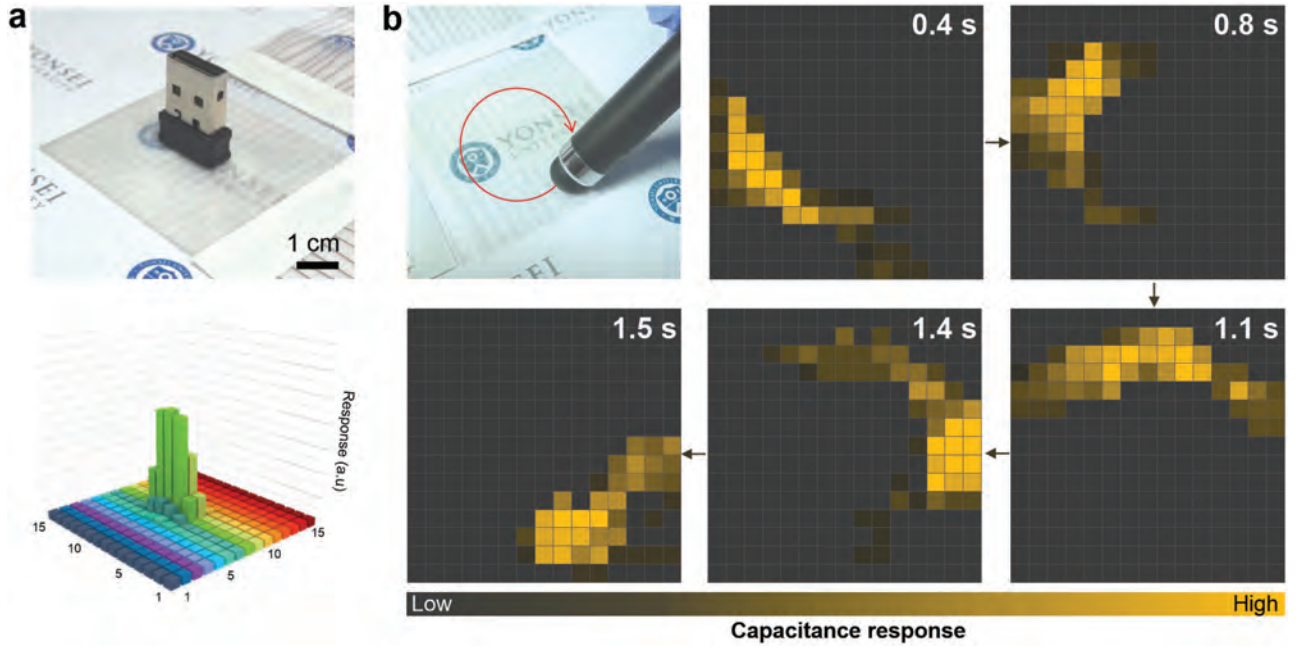

Figure 5. a) Photograph of 15 × 15 pressure sensor array fabricated using the porous structured pressure sensors (2 µm pore size) to detect spatial pressure of a wireless gender (1.66 g) and the corresponding response graph of the pressure sensor array to the external pressure. b) Real-time tactile sensing ability of the pressure sensor array for the moving direction (clockwise circle) of the pen on the pressure sensor array.

and unstructured films after loading and unloading the external load (10 kPa for 12 s). Even though the unstructured pressure sensor exhibited poor response and relaxation behaviors, with a delaying time of a few seconds and a relaxation time over 40 s to return to the original state, the porous structured pressure sensor was capable of very fast response and relaxation times when responding to external loads. In general, most materials respond to external forces in three different modes: elastic, plastic and viscoelastic behavior.[40] In the case of the viscoelastic materials, which is classified to time-dependent material, the mobilities of the polymer chain segments in the materials are significantly restricted under applied loads, because of the high density of the networks and the relatively free chain rotations, inducing the poor response of these materials to constant stresses.[41,42] Identically, the terminus of the constant loading condition, the deformed viscoelastic material is recovers gradually over long periods of time, as results of the irreversible entanglement of the polymer chains and the insufficient amount of surfaces area to store and release the elastic energy. Hence, in the case of the bare PDMS film, the critical viscoelastic behavior of the film can induce poor response and relaxation times, which severely limits its applications. However, the presence of pores in the PDMS layer drastically changes this behavior; the porous structured PDMS film exhibited rapid relaxation times (under 1 s) even under a large applied pressure of 10 kPa. Because of the pores, the porous PDMS layer has much larger deformable surfaces than the unstructured PDMS layer; this increased surface allows the porous film to be reversibly and rapidly store and release the elastic energy of the deformation imposed by the external load.[25] In addition, the porous structured pressure sensor exhibited a very rapid response time (≈40 ms) when the pressure was applied stepwise, as shown in Figure 4d; these performance parameters are comparable to those of previously reported capacitive pressure sensors.[6,19,23,38] Figure 4e shows the hysteresis curves for the porous structured pressure sensor under continuous loading and unloading cycles. Insignificant hysteresis was obtained than the unstructured pressure sensor (Figure S4, Supporting Information), indicating that the porous structured pressure sensor has excellent response stability. To evaluate the durability of the porous structured pressure sensor, its capacitive response was measured during 10 000 loading and unloading cycles. As shown in Figure 4f, the output signals of the pressure sensor exhibited negligible degradation in spite of the intensively repeated loading and unloading cyclic test, demonstrating that the porous-structured pressure sensor has high repeatability, durability, and stability under mechanical loads.

To establish the porous structured PDMS pressure sensors's ability to be used in real-time tactile sensing applications in human-computer interactions, the sensors were pixelated into a 15 × 15 array, to collect spatial pressure information. **Figure 5**a presents a photograph of the resulting pressure sensor array, with a size of 42 × 42 mm. The pressure sensor array was integrated with a Bluetooth communication circuit on a chip, and analyzed with a custom-made data acquisition system. The capacitive response of each pixel was acquired by measuring the charge-rising time in the pressure sensor pixels using the designed chip, and wirelessly transmitted to a computer. Figure 5a and Movie S1 (Supporting Information) show the use of the pressure sensor array to detect the placement of a small object (wireless receiver, 1.66 g) in a real-time sensing; the pixelated sensor array could successfully detect the spatial information of the external pressure in real-time. In addition, the real-time tactile sensing performance of the pressure sensor array was

also demonstrated with various touch shapes including several lines, and circles executed with a pen. (see Figure 5b and Movie S2, Supporting Information); as shown in Figure 5b, each pixel in the pressure sensor array exhibited a distinguishable change in capacitance, and the touch input of the clockwise circle executed with the pen could be successfully recognized in real-time based on the pressure sensor array response. It is therefore clear from these results that, the porous PDMS pressure sensor has considerable and substantial potential for real-time tactile sensor. The porous structured pressure sensor has more competitive properties compared to other capacitive pressure sensors, for instance sensitivity, response time, detection limit, and resolutions, (Table S1, Supporting Information) therefore, it can be expected to be a promising candidate in human-machine interface system development and E-skin applications.

3. Conclusion

In summary, the high-performance bioinspired porous PDMS-based pressure sensor was developed. Various porous dielectric layers with different pore sizes were successfully prepared, using multiple layers of PS beads. The porous structured pressure sensor featured a high sensitivity of 0.63 kPa^{-1} in the low-pressure region, fast response and relaxation times, an extremely low-pressure detection of 2.42 Pa (corresponding to an ant placed on top of the sensor), and excellent durability and stability properties over 10 000 working cycles. The porous structured pressure sensors were utilized to fabricate a 15 × 15 multipixel array, which was then used for real-time tactile sensing with various touch modes. Based on the outstanding performance, we believe that the bioinspired porous PDMS pressure sensor can contribute to the development of advanced pressure sensors for various applications, including E-skin, robotics, human-machine interfaces, and real-time tactile sensing systems.

4. Experimental Section

Fabrication of the Porous PDMS Pressure Sensor: A 1.2 × 1.2 cm silicon wafer was cleaned with acetone, isopropyl alcohol, and deionized water to eliminate the contaminants. An AZ1512 photoresist solution was spin-coated as a sacrificial layer on the cleaned wafers, and the sample was treated with oxygen plasma. Polystyrene latex microsphere (2.5 wt%, dispersion in water, Alfa Aesar) were dropcasted to stack multiple layers of PS beads with a face-centered cubic structure on the plasma-treated silicon wafers. After complete evaporation of the solvent of the PS beads solution, a PDMS solution prepared by mixing a prepolymer of PDMS and a curing agent (Sylgard 184; Dow Corning, USA) with a 10:1 weight composition was spin-coated on the sample and the sample was then oven heated at 80 °C for 2.5 h. After the heating process, the sample was immersed in acetone to remove the AZ1512 sacrificial layer, thus inducing the detachment of the PDMS film from the substrate. Because of the PDMS swelling issue with acetone, the PDMS film was subsequently immersed in dimethylformamide for 12 h to completely etch the PS beads, thus finalizing the porous PDMS film fabrication. The porous-structured pressure sensor was fabricated by placing the porous PDMS film between two 1 × 1.5 cm ITO/PET films (Indium tin oxide coated PET, surface resistivity 60 Ω sq^{-1}; Sigma-Aldrich).

Characterization: The surface morphologies were examined using a JEOL JSM-7001F field-emission scanning electron microscope. All capacitance measurements were taken at a frequency of 300 kHz with a 1 V AC signal, using an Agilent E4980A Precision LCR Meter. Force and frequency were controlled by an automatic *z*-axis stage loading bar with force gauge (an universal manipulator of Teraleaderm, with 0.01 N resolution). For the indentation tests, a custom-built indenter composed of two-step motors and a load cell was used. The indentation tests were conducted at 10 gf with 0.5 µm resolution; a silicon carbide ball with 1 mm the diameter was used as indentation tip.

Supporting Information

Supporting Information is available from the Wiley Online Library or from the author.

Acknowledgements

S.K. and J.L. contributed equally to this work. This work was supported by the Priority Research Centers Program (Grant No. 2009–0093823) and (No. 2014R1A2A1A11053839) through the National Research Foundation (NRF) of Korea funded by the Ministry of Education, Science and Technology (MEST) and the R&D program of MOTIE/KEIT [10064081, Development of fiber-based flexible multimodal pressure sensor and algorithm for gesture/posture-recognizable wearable devices]. The authors would like to acknowledge the support of the Ministry of Higher Education, Kingdom of Saudi Arabia for supporting this research through a grant (PCSED-009–14) under the Promising Centre for Sensors and Electronic Devices (PCSED) at Najran University, Kingdom of Saudi Arabia. Also, this work was supported by the Yonsei University Future-leading Research Initiative, Implantable artificial electronic skin for an ubiquitous healthcare system of 2016-12-0050 and Mid-career Researcher Program through NRF grant funded by the MEST (2014R1A2A2A09053061).

Received: September 6, 2016
Revised: September 28, 2016
Published online:

[1] W. Gao, S. Emaminejad, H. Y. Y. Nyein, S. Challa, K. Chen, A. Peck, H. M. Fahad, H. Ota, H. Shiraki, D. Kiriya, D.-H. Lien, G. A. Brooks, R. W. Davis, A. Javey, *Nature* **2016**, *529*, 509.
[2] M. Kaltenbrunner, T. Sekitani, J. Reeder, T. Yokota, K. Kuribara, T. Tokuhara, M. Drack, R. Schwödiauer, I. Graz, S. Bauer-Gogonea, S. Bauer, T. Someya, *Nature* **2013**, *499*, 458.
[3] J. Lee, H. Kwon, J. Seo, S. Shin, J. H. Koo, C. Pang, S. Son, J. H. Kim, Y. H. Jang, D. E. Kim, T. Lee, *Adv. Mater.* **2015**, *27*, 2433.
[4] N. Matsuhisa, M. Kaltenbrunner, T. Yokota, H. Jinno, K. Kuribara, T. Sekitani, T. Someya, *Nat. Commun.* **2015**, *6*, 7461.
[5] C. Wang, D. Hwang, Z. Yu, K. Takei, J. Park, T. Chen, B. Ma, A. Javey, *Nat. Mater.* **2013**, *12*, 899.
[6] A. P. Gerratt, H. O. Michaud, S. P. Lacour, *Adv. Funct. Mater.* **2015**, *25*, 2287.
[7] M. Park, Y. J. Park, X. Chen, Y. K. Park, M. S. Kim, J. H. Ahn, *Adv. Mater.* **2016**, *28*, 2556.
[8] W. Wu, X. Wen, Z. L. Wang, K. Takei, S. C. B. Mannsfeld, T. Someya, D. J. Lipomi, D. H. Kim, T. Sekitani, D. H. Kim, A. Javey, S. Nam, R. S. Friedman, H. Yan, C. M. Lieber, J. H. Ahn, S. Nam, X. C. Jiang, Q. H. Xiong, D. Ham, C. M. Lieber, T. Bryllert, L. E. Wernersson, L. E. Froberg, L. Samuelson, J. Zhou, W. Z. Wu, Y. G. Wei, Z. L. Wang, Z. L. Wang, Z. L. Wang, Y. Zhang, Y. Liu, Z. L. Wang, Z. L. Wang, W. Z. Wu, Z. L. Wang, J. Shi, M. B. Starr, X. D. Wang, R. S. Johansson, A. B. Vallbo, Y. G. Wei, B. Nemeth, S. A. Mascaro, H. H. Asada, Z. L. Wang, W. Z. Wu, *Science* **2013**, *340*, 952.

[9] R. S. Dahiya, G. Metta, M. Valle, G. Sandini, *IEEE Trans. Rob.* **2010**, *26*, 1.
[10] T. Sekitani, Y. Noguchi, K. Hata, T. Fukushima, T. Aida, T. Someya, *Science* **2008**, *321*, 1468.
[11] C. Pang, J. H. Koo, A. Nguyen, J. M. Caves, M. G. Kim, A. Chortos, K. Kim, P. J. Wang, J. B. H. Tok, Z. Bao, *Adv. Mater.* **2015**, *27*, 634.
[12] R. C. Webb, A. P. Bonifas, A. Behnaz, Y. Zhang, K. J. Yu, H. Cheng, M. Shi, Z. Bian, Z. Liu, Y.-S. Kim, W.-H. Yeo, J. S. Park, J. Song, Y. Li, Y. Huang, A. M. Gorbach, J. A. Rogers, *Nat. Mater.* **2013**, *12*, 938.
[13] H.-H. Chou, A. Nguyen, A. Chortos, J. W. F. To, C. Lu, J. Mei, T. Kurosawa, W.-G. Bae, J. B.-H. Tok, Z. Bao, *Nat. Commun.* **2015**, *6*, 8011.
[14] Q. Shao, Z. Niu, M. Hirtz, L. Jiang, Y. Liu, Z. Wang, X. Chen, *Small* **2014**, *10*, 1466.
[15] B. Zhu, Z. Niu, H. Wang, W. R. Leow, H. Wang, Y. Li, L. Zheng, J. Wei, F. Huo, X. Chen, *Small* **2014**, *10*, 3625.
[16] B. Zhu, H. Wang, Y. Liu, D. Qi, Z. Liu, H. Wang, J. Yu, M. Sherburne, Z. Wang, X. Chen, *Adv. Mater.* **2016**, *28*, 1559.
[17] D. J. Lipomi, M. Vosgueritchian, B. C.-K. Tee, S. L. Hellstrom, J. a. Lee, C. H. Fox, Z. Bao, *Nat. Nanotechnol.* **2011**, *6*, 788.
[18] J. A. Dobrzynska, M. A. M. Gijs, *Sens. Actuators, A* **2012**, *173*, 127.
[19] B. Nie, R. Li, J. Cao, J. D. Brandt, T. Pan, *Adv. Mater.* **2015**, *27*, 6055.
[20] M. H. Zhao, Z. L. Wang, S. X. Mao, *Nano Lett.* **2004**, *4*, 587.
[21] L. Persano, C. Dagdeviren, Y. Su, Y. Zhang, S. Girardo, D. Pisignano, Y. Huang, J. a. Rogers, *Nat. Commun.* **2013**, *4*, 1633.
[22] M. Rothmaier, M. P. Luong, F. Clemens, *Sensors* **2008**, *8*, 4318.
[23] B. C. K. Tee, A. Chortos, R. R. Dunn, G. Schwartz, E. Eason, Z. Bao, *Adv. Funct. Mater.* **2014**, *24*, 5427.
[24] S. Park, H. Kim, M. Vosgueritchian, S. Cheon, H. Kim, J. H. Koo, T. R. Kim, S. Lee, G. Schwartz, H. Chang, Z. Bao, *Adv. Mater.* **2014**, *26*, 7324.
[25] S. C. B. Mannsfeld, B. C.-K. Tee, R. M. Stoltenberg, C. V. H.-H. Chen, S. Barman, B. V. O. Muir, A. N. Sokolov, C. Reese, Z. Bao, *Nat. Mater.* **2010**, *9*, 859.
[26] L. Y. Li, Y. F. Dong, W. F. Jiang, H. F. Ji, X. J. Li, *Thin Solid Films* **2008**, *517*, 948.
[27] S. Miller, Z. Bao, *J. Mater. Res.* **2015**, *3*, 3584.
[28] T. Takahashi, M. Suzuki, S. Iwamotoi, S. Aoyagi, *Micromachines* **2012**, *3*, 270.
[29] J. Wang, J. Jiu, M. Nogi, T. Sugahara, S. Nagao, H. Koga, P. He, K. Suganuma, *Nanoscale* **2015**, *7*, 2926.
[30] D. Kang, P. V. Pikhitsa, Y. W. Choi, C. Lee, S. S. Shin, L. Piao, B. Park, K.-Y. Suh, T. Kim, M. Choi, *Nature* **2014**, *516*, 222.
[31] G. Y. Bae, S. W. Pak, D. Kim, G. Lee, D. H. Kim, Y. Chung, K. Cho, *Adv. Mater.* **2016**, *28*, 5300.
[32] M. Kolle, A. Lethbridge, M. Kreysing, J. J. Baumberg, J. Aizenberg, P. Vukusic, *Adv. Mater.* **2013**, *25*, 2239.
[33] J. Yang, J. Chen, Y. Su, Q. Jing, Z. Li, F. Yi, X. Wen, Z. Wang, Z. L. Wang, *Adv. Mater.* **2015**, *27*, 1316.
[34] F. Natalio, T. P. Corrales, M. Panthofer, D. Schollmeyer, I. Lieberwirth, W. E. G. Muller, M. Kappl, H.-J. Butt, W. Tremel, *Science* **2013**, *339*, 1298.
[35] G. Duan, S. Jiang, V. Jérôme, J. H. Wendorff, A. Fathi, J. Uhm, V. Altstädt, M. Herling, J. Breu, R. Freitag, S. Agarwal, A. Greiner, *Adv. Funct. Mater.* **2015**, *25*, 2850.
[36] A. V. Ereskovsky, *The Comparative Embryology of Sponges*, Springer Science & Business Media, Berlin, Germany **2010**.
[37] S. M. Miriyala, Y. S. Kim, L. Liu, J. C. Grunlan, *Macromol. Chem. Phys.* **2008**, *209*, 2399.
[38] T. Li, H. Luo, L. Qin, X. Wang, Z. Xiong, H. Ding, Y. Gu, Z. Liu, T. Zhang, *Small* **2016**, *12*, 5042.
[39] H. Zhang, B. E. Schuster, Q. Wei, K. T. Ramesh, *Scr. Mater.* **2006**, *54*, 181.
[40] W. N. N. Findley, J. S. S. Lai, K. Onaran, *Creep and Relaxation of Nonlinear Viscoelastic Materials: With an Introduction to Linear Viscoelasticity*, Elsevier, Amsterdam, The Nederlands **2012**.
[41] R. J. Messinger, T. G. Marks, S. S. Gleiman, F. Milstein, B. F. Chmelka, *Macromolecules* **2015**, *48*, 4835.
[42] J. William, D. Callister, *Fundamentals of Materials Science and Engineering*, John Wiley & Sons, Hoboken, NJ, USA **2012**.